

Received July 11, 2019, accepted July 30, 2019, date of publication August 1, 2019, date of current version August 20, 2019.

Digital Object Identifier 10.1109/ACCESS.2019.2932576

# Experimental Investigation of Millimeter-Wave MIMO Channel Characteristics in Tunnel

XI LIU<sup>1</sup>, XIAOYU YIN<sup>1</sup>, AND GUOXIN ZHENG

Key Laboratory of Specialty Fiber Optics and Optical Access Networks, Joint International Research Laboratory of Specialty Fiber Optics and Advanced Communication, Shanghai Institute for Advanced Communication and Data Science, Shanghai University, Shanghai 200072, China

Corresponding author: Guoxin Zheng (gxzheng@staff.shu.edu.cn)

This work was supported by the National Natural Science Foundation of China under Grant 61871261.

**ABSTRACT** A 28 GHz millimeter-wave (mm-wave) propagation measurement campaign was performed to predict the multiple-input multiple-output (MIMO) channel performance in a tunnel environment. Two kinds of polarization configurations were studied in this paper. In order to overcome the serious path loss (PL) of mm-wave propagation, a high gain directional horn antenna was used in the measurements of tunnel environment. The measurement results and simulation results at same specific locations are compared. The result of comparison indicates that the simulation model matches the measurement well. Then the MIMO capacity at other locations of the tunnel can be predicted by the simulation model. Further-more, it is inferred that the antenna array elements of horizontally polarized configuration have higher capacity than the vertically polarized under the constant signal-to-noise ratio (SNR).

**INDEX TERMS** Channel, multiple-input multiple-output (MIMO), millimeter-wave (mm-wave), tunnel.

## I. INTRODUCTION

There is now a growing interest in the urban rail transit systems in underground tunnels to increase the data rates. While the reality of a spectrum shortfall is now rapidly increasing [1]. To address this challenge, there has been found an emerging attention in the so-called millimeter-wave (mm-wave) bands, which has a massive amount of raw bandwidth.

Understanding of wireless channel characteristics is very important for the designing of wireless communication systems. So it is essential to study the mm-wave multiple-input multiple-output (MIMO) channel propagation characteristics in subway tunnels. MIMO channel performance was initially investigated in the subway tunnel environment in [2] for the lower frequency band (under 6 GHz). Afterwards, the theory of MIMO studies based on modal analysis and experimental campaigns have been performed for subway tunnels [3], [4].

To the best of our knowledge, only a few papers [5]–[7] are focused on the ‘non-subway’ tunnels (mine tunnels) at 60 GHz frequency band. In [5], Single-input single-output (SISO) mm-wave channel measurements were conducted in a mine tunnel under the narrow and wide environments. The results show that the capacity of SISO channel in narrow

environment is higher than that in wide environment, and its path loss (PL) exponent is found lower than that in the free space. In [6], a measurement campaign was performed in a mine tunnel and  $2 \times 2$  mm-wave MIMO channel capacity using microstrip patch antenna arrays was calculated for the line of sight (LOS) and non-LOS (NLOS) conditions. A mm-wave MIMO channel measurement using high gains directional horn antenna in the same mine tunnel were executed in [7]. Since the dimension, material or roughness of the wall in mine tunnel are quite different from the subway tunnel, so here we performed the MIMO channel measurements in the Nantong tunnel in Zhongtian technology company (ZTT), Nantong, China at 28 GHz. Moreover, we used these measurement results to predict the mm-wave MIMO channel performance in a subway tunnel.

The rest of this paper is organized as follows. Section II explains the measurement and the simulation setup and procedure. Experimental results and simulation results are studied and analyzed in section III. Finally, section IV depicts the conclusions.

## II. MEASUREMENT AND SIMULATION ENVIRONMENT AND SETUP

### A. MEASUREMENT

The measurements were conducted in the subway-like tunnel in ZTT, Nantong, China and the inner scenario is shown

The associate editor coordinating the review of this manuscript and approving it for publication was Cesar Briso.

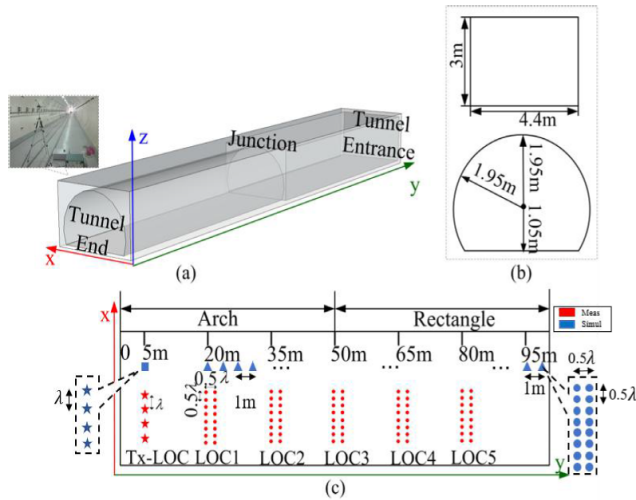


FIGURE 1. Nantong tunnel and Tx-Rx arrays locations [8].

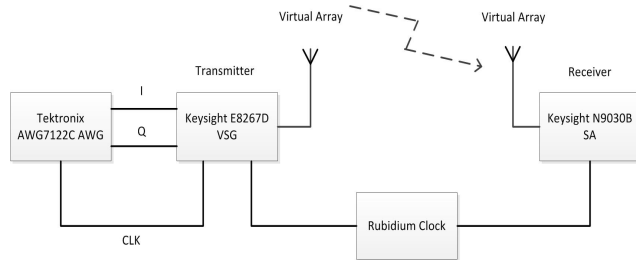


FIGURE 2. Channel sounding setup.

TABLE 1. Channel measurement parameters.

| DESCRIPTION        | Value       |
|--------------------|-------------|
| center frequency   | 28 GHz      |
| transmit power     | 23 dBm      |
| bandwidth          | 100 MHz     |
| sample rate        | 200 MHz     |
| Delay resolution   | 10 ns       |
| Maximum delay      | 5110 ns     |
| Transmit signal    | PN sequence |
| PN sequence length | 511 chips   |
| Tx antenna height  | 1.6 m       |
| Rx antenna height  | 1.6 m       |

in Fig. 1 and the sounding setup is shown in Fig. 2. The measurement parameters are summarized in Table 1. The detailed information of the measurement environment and sounding setup can be found in our previous work [8]. The virtual array was used to realize the MIMO measurement.

Two types of polarization configurations (VV, HH) were considered during the measurements. The directional antenna was used as a horn antenna whose half-power beam width is 16° and the gain is 19.25 dBi. Vertically polarized transmitting/receiving signals can be realized by placing vertically the long side of the antenna aperture to the ground, and further rotating it with 90° parallel to the ground for realizing horizontally polarized transmitting/ receiving signals.

VV: All Tx and Rx antenna array elements are vertically polarized.

HH: All Tx and Rx antenna array elements are horizontally polarized.

TABLE 2. Properties of the tunnel wall used in wireless insite.

| Material | Thickness(m) | Roughness | Conductivity(s/m) | Permittivity |
|----------|--------------|-----------|-------------------|--------------|
| concrete | 0.5          | 0.001     | 0.48              | 5.31         |

B. SIMULATION

We use Wireless InSite ray-tracing software to obtain simulation results. The simulation 3-D model is established according to the measurement environment by AutoCAD. The 100 m long tunnel is consisted of 50 m rectangular part and 50 m arch part. The width and height of the tunnel is 4.4 m and 3 m, respectively. The configurations of walls are shown in Table 2. To investigate MIMO capacity on other locations, a further simulation in which the Tx-Rx distance range is from 15 m to 94m in with 1 m interval as is shown in Fig. 1.

III. DATA PROCESSING AND ANALYSIS

The CIR is directly generated by the cross-correlation of the collected data with the replica of the transmitted sequence [9]. To separate the valid multipath components (MPCs) from the background noise, the threshold value was calculated based on a 5 dB signal-to-noise ratio (SNR) threshold relative to the mean thermal noise floor of the raw power delay profile [1].

Mutual information capacity is a fundamental property of a MIMO-based system. To calculate the MIMO channel capacity, (1) was used to get the narrow band channel impulse response [10].

$$h_{narr}(t, s, u) = \sum_{i=1}^{N_\tau} \tilde{h}(t, \tau_i, s, u) \tag{1}$$

where  $N_\tau$  is the number of multipath,  $s$  denotes the  $s$ -th Rx antenna and is the  $u$ -th Tx antenna.

It is a common practice to normalize the MIMO channel matrices before analyzing the MIMO channel capacity. The normalized channel matrix for each channel realization is expressed as [11]

$$\mathbf{H}_{nor} = \mathbf{H} \sqrt{\frac{N_{Tx} N_{Rx}}{\|\mathbf{H}\|_F^2}} \tag{2}$$

where  $\|\mathbf{H}\|_F$  denotes Frobenius norm, and it is given by

$$\|\mathbf{H}\|_F = \sqrt{\sum_{i=1}^{N_{Rx}} \sum_{j=1}^{N_{Tx}} |h_{ij}|^2} \tag{3}$$

Assuming no channel state information is available at the Tx, so the capacity of the MIMO channel can be calculated as

$$C = \log_2 \left[ \det \left( \mathbf{I}_{N_{Rx}} + \frac{\rho}{N_{Tx}} \mathbf{H}_{nor} \mathbf{H}_{nor}^* \right) \right] \tag{4}$$

where  $\rho$  is the average SNR,  $(\bullet)^*$  denotes the Hermitian transpose of a matrix,  $N_{Tx}$  and  $N_{Rx}$  are the number of Tx and Rx antenna elements, respectively.  $\mathbf{I}_{N_{Rx}}$  is the identity matrix of size  $N_{Rx} \times N_{Rx}$ .

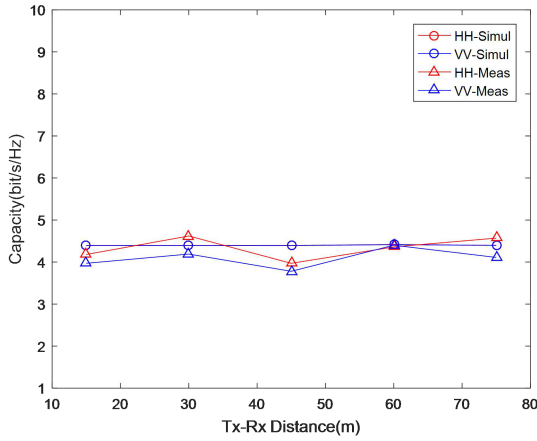


FIGURE 3. 2 × 2 MIMO capacity against Tx-Rx distance for a constant SNR of 10 dB.

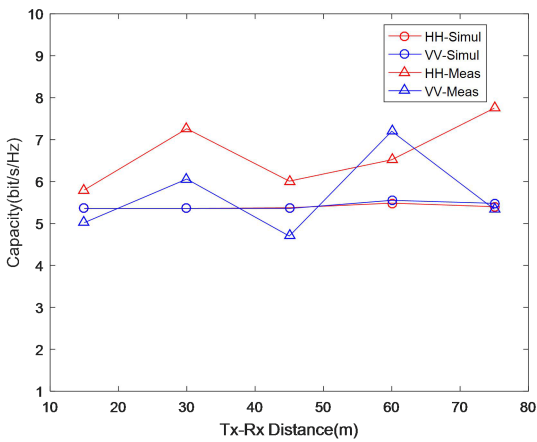


FIGURE 4. 4 × 4 MIMO capacity against Tx-Rx distance for a constant SNR of 10 dB.

**A. MIMO CHANNEL CAPACITY FOR A CONSTANT SNR WITH COMPARISON BETWEEN MEASUREMENT AND SIMULATION**

In order to perform a fair comparison of different systems or schemes, a constant SNR of 10 dB was considered. The 2 × 2 and 4 × 4 MIMO channel capacity for a constant SNR is given in Fig. 3 and Fig. 4, correspondingly. The simulation results are lower than measurement results in the figures. Since the simulation is an ideal environment, there are some small scatters on the wall during the measurement that are not considered in simulation, so the simulation results are lower than the measured results. The simulation results have the same trend as the measurement results in spite of the location at 30 m. The reason caused the difference between measurement and simulation is that the measurement environment has metallic materials on the location of 30 m which causes strong reflection. MIMO capacity in measurement is higher near this location than simulation. So we can conclude that the simulation model meets the measurement well. The mean capacity of all Tx-Rx distance for HH and VV is given in Table 3. It is observable that the HH performed better than the VV.

TABLE 3. Mean capacity for a constant SNR of 10 dB(5locs).

| Polarization configuration | Average Capacity (bit/s/Hz) |      |      |
|----------------------------|-----------------------------|------|------|
|                            | 4×4                         | 2×2  | SISO |
| VV-Meas                    | 5.7                         | 4.1  | 3.5  |
| HH-Meas                    | 6.7                         | 4.3  | 3.5  |
| VV-Simul                   | 5.42                        | 4.39 | 3.46 |
| HH-Simul                   | 5.40                        | 4.39 | 3.46 |

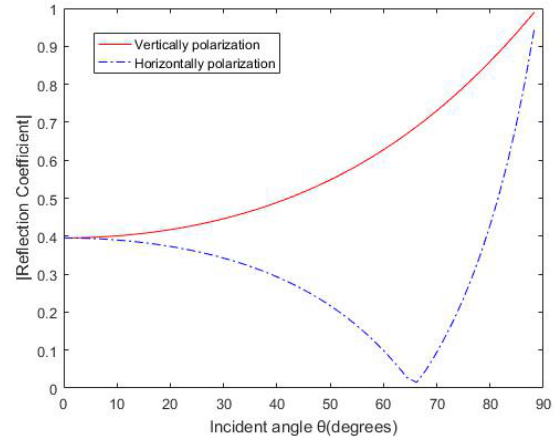


FIGURE 5. Reflection coefficient of vertically and horizontally polarized signals.

The reason caused the phenomenon above is illustrated as follows. The conductivity and relative dielectric constant of concrete are 0.48 S/m and 5.31 according to the International Telecommunication Union (ITU) recommendations at 28 GHz. For reflections on non-perfectly conducting surfaces, the plane wave Fresnel reflection coefficients for vertical polarization ( $\perp$ ) and horizontal polarization ( $\parallel$ ) are given by [12]

$$R_{\perp}(\theta) = \frac{\cos(\theta) - \sqrt{\epsilon' - \sin^2(\theta)}}{\cos(\theta) + \sqrt{\epsilon' - \sin^2(\theta)}} \quad (5)$$

and

$$R_{\parallel}(\theta) = \frac{\epsilon' \cos(\theta) - \sqrt{\epsilon' - \sin^2(\theta)}}{\epsilon' \cos(\theta) + \sqrt{\epsilon' - \sin^2(\theta)}} \quad (6)$$

where  $\epsilon' = \epsilon/\epsilon_0 - j\sigma/(\omega\epsilon_0)$ ,  $\omega = 2\pi f$ , with  $\epsilon = \epsilon_r\epsilon_0$  the permittivity of the material,  $\sigma$  the conductivity,  $\epsilon_r$  the relative dielectric constant,  $\epsilon_0$  is a constant of  $8.85 \times 10^{-12}$  F/m,  $f$  is the carrier frequency and  $\theta$  the incidence angle. The reflection coefficients of vertical and horizontal polarizations are varying with incident angle as given in Fig. 5. As can be seen, vertical polarization coefficient increases with the incidence angle. But horizontal polarization coefficient has a Brewster angle, and is always lower than the vertical polarization coefficient.

For horizontally polarized signals, the incident ray on the tunnel ceiling and floor is horizontally polarized but vertical polarization is observed on the tunnel walls. For vertically polarized signals, the opposite response is observed. According to the reflection coefficient, the reflection ray power on the tunnel wall for HH is larger than the VV. Because the

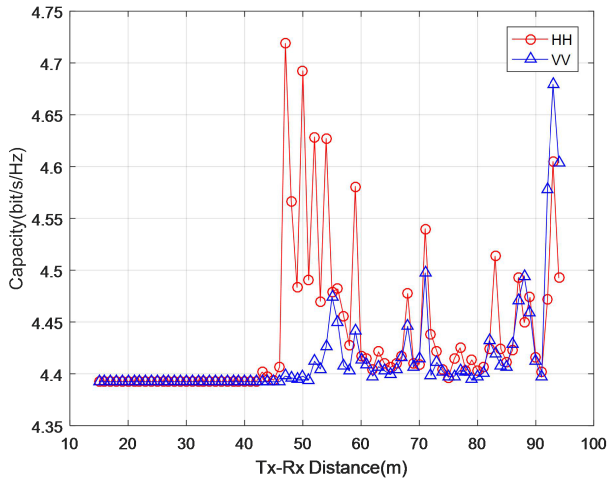


FIGURE 6. 2 × 2 MIMO capacity against Tx-Rx distance with prediction for a constant SNR of 10 dB.

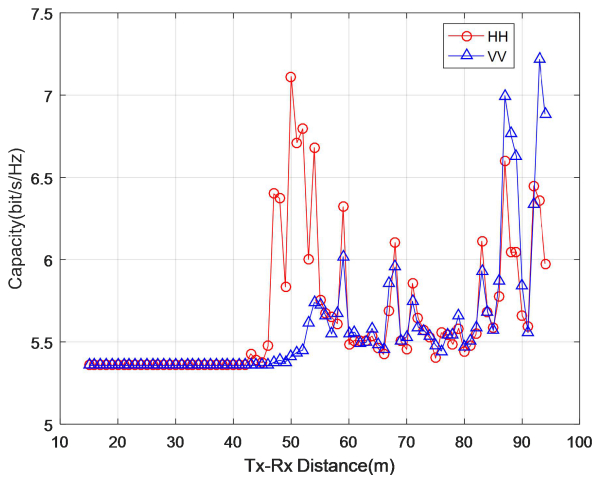


FIGURE 7. 4 × 4 MIMO capacity against Tx-Rx distance with prediction for a constant SNR of 10 dB.

tunnel width is larger than the tunnel height, the reflected rays on the tunnel walls have larger angle of arrival than tunnel ceiling and floor. This results in a higher angular spread for HH than the VV. So the HH configuration has larger channel capacity than the VV configuration.

**B. MIMO CHANNEL CAPACITY FOR A CONSTANT SNR WITH COMPARISON BETWEEN MEASUREMENT AND SIMULATION**

To investigate MIMO capacity on other locations of the tunnel. The simulation with 80 receivers’ locations is done. Each location has 2 × 8 = 16 antennas. The Tx-Rx distance ranges from 15 m to 94 m and the interval between two locations is 1 m. The predicted 2 × 2 and 4 × 4 MIMO channel capacity with constant SNR are shown in Fig. 6 and Fig. 7, respectively.

The MIMO channel capacity of HH and VV is almost overlapped when Tx-Rx distance ranges from 15m to 45m due to high Ricean *K* factor, which is defined as the power ratio of LOS components and NLOS components. As can

TABLE 4. Mean capacity with prediction for a constant SNR of 10 dB(80locs).

| Polarization Configuration | Average Capacity (bit/s/Hz) |       |      |
|----------------------------|-----------------------------|-------|------|
|                            | 4 × 4                       | 2 × 2 | SISO |
| VV                         | 5.59                        | 4.41  | 3.46 |
| HH                         | 5.65                        | 4.44  | 3.46 |

be seen in Fig. 6 and Fig. 7, MIMO channel capacity of the HH and the VV under a constant SNR of 10 dB increase when Tx-Rx distance ranges from 45m to 95m due to the decrease of *K* factor and the HH is higher than that of VV. The mean capacity of all Tx-Rx distance for HH and VV is given in Table 4. The prediction results show that the HH has a higher mean capacity than the VV. So, the HH is suggested to be a better polarization configuration for the future mm-wave MIMO communication in the tunnel. Since a MIMO system is quite complicated, it is rather important to compare its performance with a SISO system. As displayed in Table 3 and Table 4, whether it is actual measurement or simulation, the mean capacities of the 2 × 2 MIMO and 4 × 4 MIMO systems are higher than that of the SISO system.

**IV. CONCLUSION**

The mm-wave MIMO channel measurement at 28 GHz by using directional antennas was performed in a subway tunnel in Nantong, China. In order to overcome the high attenuation at the mm-wave frequency band, the high gain directional pyramidal horn antenna was used in the measurements. Two polarization configurations (VV, HH) were considered in these measurements. In summary this study concludes as follows:

- The simulation results of mean MIMO capacity is lower than the measurements because of more scatters in measurement environment that cause strong reflection which simulation can’t totally simulate.
  - In a subway tunnel, the capacity of HH is higher than the VV for a constant SNR either in measurement or simulation.
- Therefore, for mm-wave MIMO in tunnel, HH is a better polarization configuration for the future mm-wave MIMO communication systems in subway tunnels.

**REFERENCES**

- [1] T. S. Rappaport, G. R. MacCartney, M. K. Samimi, and S. Sun, “Wideband millimeter-wave propagation measurements and channel models for future wireless communication system design,” *IEEE Trans. Commun.*, vol. 63, no. 9, pp. 3029–3056, Sep. 2015.
- [2] M. Lienard, P. Degauque, J. Baudet, and D. Degardin, “Investigation on MIMO channels in subway tunnels,” *IEEE J. Sel. Areas Commun.*, vol. 21, no. 3, pp. 332–339, Apr. 2003.
- [3] J. M. Molina-Garcia-Pardo, M. Lienard, P. Degauque, D. G. Dudley, and L. Juan-Llacer, “Interpretation of MIMO channel characteristics in rectangular tunnels from modal theory,” *IEEE Trans. Veh. Technol.*, vol. 57, no. 3, pp. 1974–1979, May 2008.
- [4] J. M. Molina-Garcia-Pardo, M. Lienard, P. Degauque, C. Garcia-Pardo, and L. Juan-Llacer, “MIMO channel capacity with polarization diversity in arched tunnels,” *IEEE Antennas Wireless Propag. Lett.*, vol. 8, pp. 1186–1189, 2009.
- [5] M. E. Khaled, P. Fortier, and M. L. Ammari, “A performance study of line-of-sight millimeter-wave underground mine channel,” *IEEE Antennas Wireless Propag. Lett.*, vol. 13, pp. 1148–1151, 2014.

- [6] I. B. Mabrouk, J. Hautcoeur, L. Talbi, M. Nedil, and K. Hettak, "Feasibility of a millimeter-wave MIMO system for short-range wireless communications in an underground gold mine," *IEEE Trans. Antennas Propag.*, vol. 61, no. 8, pp. 4296–4305, Aug. 2013.
- [7] M. Ghaddar, L. Talbi, M. Nedil, I. B. Mabrouk, T. A. Denidni, "Mm-waves propagation measurements in underground mine using directional MIMO antennas," *IET Microw. Antennas Propag.*, vol. 10, no. 5, pp. 517–524, Apr. 2016.
- [8] X. Yin, X. Liu, G. Zheng, A. Saleem, and X. Zhai, "28-GHz channel characterization for a short tunnel," *IEEE Microw. Wireless Compon. Lett.*, vol. 28, no. 12, pp. 1146–1148, Dec. 2018.
- [9] P. Truffer and P. E. Leuthold, "Wide-band channel sounding at 24 GHz based on a novel fiber-optic synchronization concept," *IEEE Trans. Microw. Theory Techn.*, vol. 49, no. 4, pp. 692–700, Apr. 2001.
- [10] A. Boettcher, C. Schneider, M. Narandzic, P. Vary, and R. S. Thomae, "Power and delay domain parameters of channel measurements at 2.53 GHz in an Urban macro cell scenario," in *Proc. 4th Eur. Conf. Antennas Propag.*, Apr. 2010, pp. 1–5.
- [11] I. B. Mabrouk, L. Talbi, M. Nedil, Y. Coulibaly, and T. A. Denidni, "Effect of antenna directivity on performance of multiple input multiple output systems in an underground gold mine," *IET Microw. Antennas Propag.*, vol. 6, no. 5, pp. 555–561, Apr. 2012.
- [12] F. P. Fontaen, and P. M. Espiãeira, *Modelling the Wireless Propagation Channel: A Simulation Approach With Matlab*. Hoboken, NJ, USA: Wiley, 2008.



**XIAOYU YIN** received the B.S., M.S., and Ph.D. degrees in communication and information system from Shanghai University, China, in 2010, 2013, and 2018, respectively. His research interests include wireless channel modeling and channel measurement on millimeter-wave (mm-wave) frequency band in confined area. His other works on the research of millimeter-wave have been published on other famous journals and conference such as *IET Microwaves, Antennas & Propagation, High Technology Letters*, and *ICCP*.



**XI LIU** received the B.Eng. and M.Eng. degrees from Shanghai University, Shanghai, China, in 2008 and 2010, respectively, where he is currently pursuing the Ph.D. degree in communication and information engineering. He worked in the areas of railway and metro wireless channel modeling and mobile communications. He has been with the China Railway Shanghai Design Institute Group Co., Ltd., as the Deputy Chief Engineer, since 2008. Over the past three years, he has completed more than 15 scientific research projects sponsored by the National Natural Science Foundation of China, government, and enterprises. In the study of railway and metro wireless channel, he received the Science and Technology Progress Award twice from China Railway Construction Co., Ltd., in 2015 and 2017.



**GUOXIN ZHENG** received the B.Eng. and M.Eng. degrees from Taiyuan Science and Technology University, China, in 1982 and 1987, respectively. He worked in the area of wireless channel modeling and mobile communications. He has been with Shanghai University as a Full Professor since 2000. Over the past five years, he has completed more than 20 scientific research projects sponsored by the National Natural Science Foundation of China, the Shanghai Municipal Government and enterprises. In the study of metro wireless channel, he received the Shanghai Science and Technology Progress Award twice in 2010 and 2014.

...